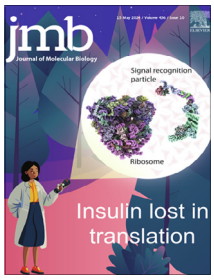

MutL Activates UvrD by Interaction Between the MutL C-terminal Domain and the UvrD 2B Domain

Olha Storozhuk [1,†], Susanne R. Bruekner [2], Ankon Paul [3], Joyce H. G. Lebbink [3,4], Titia K. Sixma [2] and Peter Friedhoff [1,*]

*1 - **Institute for Biochemistry,** FB 08, Justus Liebig University, Heinrich-Buff-Ring 17, D-35392 Giessen, Germany*
*2 - **Division of Biochemistry,** Netherlands Cancer Institute and Oncode Institute, Amsterdam, the Netherlands*
*3 - **Department of Molecular Genetics,** Oncode Institute, Erasmus MC Cancer Institute, Erasmus University Medical Center, Rotterdam, the Netherlands*
*4 - **Department of Radiotherapy,** Erasmus University Medical Center, Rotterdam, the Netherlands*

***Correspondence to Peter Friedhoff:** Peter.Friedhoff@chemie.bio.uni-giessen.de (P. Friedhoff)*
https://doi.org/10.1016/j.jmb.2024.168589
Edited by Dylan Taatjes

Abstract

UvrD is a helicase vital for DNA replication and quality control processes. In its monomeric state, UvrD exhibits limited helicase activity, necessitating either dimerization or assistance from an accessory protein to efficiently unwind DNA. Within the DNA mismatch repair pathway, MutL plays a pivotal role in relaying the repair signal, enabling UvrD to unwind DNA from the strand incision site up to and beyond the mismatch. Although this interdependence is well-established, the precise mechanism of activation and the specific MutL-UvrD interactions that trigger helicase activity remain elusive. To address these questions, we employed site-specific crosslinking techniques using single-cysteine variants of MutL and UvrD followed by functional assays. Our investigation unveils that the C-terminal domain of MutL not only engages with UvrD but also acts as a self-sufficient activator of UvrD helicase activity on DNA substrates with 3′-single-stranded tails. Especially when MutL is covalently attached to the 2B or 1B domain the tail length can be reduced to a minimal substrate of 5 nucleotides without affecting unwinding efficiency.

Introduction

The correction of misincorporated bases during replication is an essential process for maintaining genome integrity in all living organisms. Lack thereof leads to a mutator phenotype in bacteria and cancer in higher organisms.[1,2] The main system that ensures the correction of errors is DNA mismatch repair (MMR).[3,4] Base-base mismatches or short insertion or deletion loops are recognized, removed, and the correct DNA sequence resynthesized. This process is conserved from *E. coli* to humans, underscoring its importance for genome maintenance.

In *E. coli*, MutS scans the DNA after replication and detects and binds to mismatches.[5–7] Upon ATP binding, MutS changes conformation, releasing the mismatch and recruiting the homodimeric MutL onto the DNA.[8–11] Once activated and bound to DNA, MutL enables several downstream events in MMR. In a first step, it promotes the generation of a nick in the newly synthesized strand at hemimethylated GATC sites by binding and activating the latent endonuclease MutH.[12–14] Subsequently, MutL activates UvrD (DNA helicase II), initiating the unwinding of DNA between the incision site and the mismatch.[15–18] This allows for the degradation of the strand up to and including the

erroneously incorporated nucleotide by one of several exonucleases.[19] Interestingly, exonuclease-independent mismatch repair is not only occurring in eukaryotes,[20,21] but has also recently been proposed to occur in *E. coli* through MutL-mediated helicase-driven removal of DNA fragments that are flanked by multiple nicks.[22] Multiple nicks were previously shown to enhance mismatch repair efficiency both in *E. coli* and human mismatch repair.[23] Helicase-driven gap creation is followed by resynthesis by polymerase and sealing of the remaining nick by ligase.[3,24,25] MutL is a 70 kDa GHKL ATPase composed of two globular domains, the 40 kDa N-terminal domain ($MutL^{LN40}$, residues 1–349) and the 20 kDa C-terminal domain ($MutL^{LC20}$, residues 428–615), connected by a non-conserved linker (Figure 1A).[26] MutL forms a homodimer through the dimerization domain (residue 433–478, 570–615) in $MutL^{LC20}$,[26–28] while the flanking domain in $MutL^{LC20}$ is referred to as the regulatory domain (residues 479–567).[29] Upon ATP binding, the N-terminal domains of MutL can also interact to form a closed conformation,[30] encircling the DNA. A natural thrombin cleavage site has been used to split the protein into $MutL^{LN40}$ and a longer C-terminal fragment named $MutL^{LC30}$ (residues 350–615) (Figure 1A).[31] MutL homologs exhibit extreme flexibility that is modulated by adenine nucleotide, which has been investigated biochemically and biophysically (e.g., by gel filtration, dynamic light scattering).[30] Atomic force microscopy studies of the eukaryotic MutL homologs revealed a great variety of conformations ranging from extended, one-armed, closed, or condensed conformations.[32] To understand the roles of the MutL domains and to capture transient interactions in previous studies, we had generated single-cysteine variants of MutL that were active both *in vitro* and *in vivo*.[28,33] For example, the atomic structures of the complex between MutS and $MutL^{LN40}$ could be obtained only after site-specific crosslinking using single-cysteine variants of both proteins.[5,8]

UvrD is an 80 kDa SF1 helicase involved not only in MMR but also in nucleotide excision repair,[34] homologous recombination[35] and rolling circle replication.[36] UvrD utilizes the energy of ATP hydrolysis to translocate along single-stranded DNA (ssDNA) in a 3′–5′ direction, leading to the unwinding of double stranded DNA.[37–39] *In vitro*, UvrD can function as a monomer[40] or as a dimer[41] with monomeric UvrD sufficient for translocation along ssDNA[42] and dimeric or accessory protein-activated UvrD required for DNA unwinding.[39,43] UvrD can initiate unwinding from various DNA structures, including gaps, nicks, double-strand/single-strand junction with a 3′ single-strand DNA (3′ ssDNA) tail, and to some extent also blunt ends.[44,45] The length of the 3′ ssDNA tail in double-strand/single-strand junctions significantly influence UvrD's efficiency. While UvrD monomers can tightly bind to junctions with a 3′ ssDNA tail of at least 4 nucleotides (nt), helicase activity is observed from 3′ ssDNA tail lengths of 12 nt, consistent with the model of an active UvrD dimer.[46] Additionally, for unwinding stimulation by MutL, the length of the 3′ ss-DNA tail must be at least 10 nt.[47] These findings suggested that both the second UvrD or MutL interact with a portion of the 3′ ssDNA tail.[47]

UvrD comprises four domains (1A, 1B, 2A and 2B) forming the core of the protein, along with a small Tudor domain connected at the C-terminus by a flexible linker (Figure 1B).[48,49] The Tudor domain has been found to facilitate the interaction with RNA-polymerase and Ku protein.[50–52] Crystallographic studies revealed different conformations of UvrD, with the 2B domain undergoing large changes in orientation between apo and DNA-bound states.[53] In the apo structure, the 2B domain adopts an open state, tilted away from the 1B domain (Figure 1B left panel),[54] while the DNA and ADP-MgF_3-bound structure shows a closed state, with the 2B domain rotated (Figure 1B right panel).[48] Single-molecule Förster resonance energy transfer (FRET) experiments with UvrD labelled on the $UvrD^{2B}$ and $UvrD^{1B}$ domain suggest the existence of intermediate states in solution.[55,56] It has been shown that actively unwinding UvrD adopts a state resembling an intermediate state of the open and closed states observed in the crystal structure[56–58] and that dimerization of UvrD or interaction with MutL induces this state and enhances helicase activity.[54,56]

The specific interaction surface between MutL on UvrD is not known, but the $UvrD^{2B}$ domain is crucial for their interaction and activation.[56] MutL likely prevents autoinhibition by the $UvrD^{2B}$ domain, as observed in the related Rep helicase.[59,60] MutL is believed to travel together with UvrD and lower UvrD's dissociation rate from DNA.[47] Previous studies have identified crosslinks between lysine residues in $MutL^{LC30}$ (residues 351–615) and UvrD, as well as between $MutL^{LC30}$ and $MutL^{LN40}$ (residues 1–314) and UvrD, using bis-sulfosuccinimidyl suberate (BS^3) crosslinking reagent in the absence or presence of DNA and AMPPNP, respectively.[26] Additionally, yeast two-hybrid assays demonstrated that a C-terminal fragment of MutL (residues 398–615) is sufficient for interaction with UvrD,[17] although the relevance of this interaction for UvrD helicase activation remains unclear as a C-terminal fragment (i.e., $MutL^{LC24}$, residues 394–615) alone was unable to activate the UvrD helicase.[26]

Here, we conducted site-specific crosslinking experiments using different single-cysteine variants of MutL and UvrD to investigate their interactions and assess the impact on the DNA unwinding activity. Our findings demonstrate that the single cysteines in the C-terminal domain of MutL form crosslinks to single cysteines in UvrD, particularly in the UvrD 2B domain. Notably, the

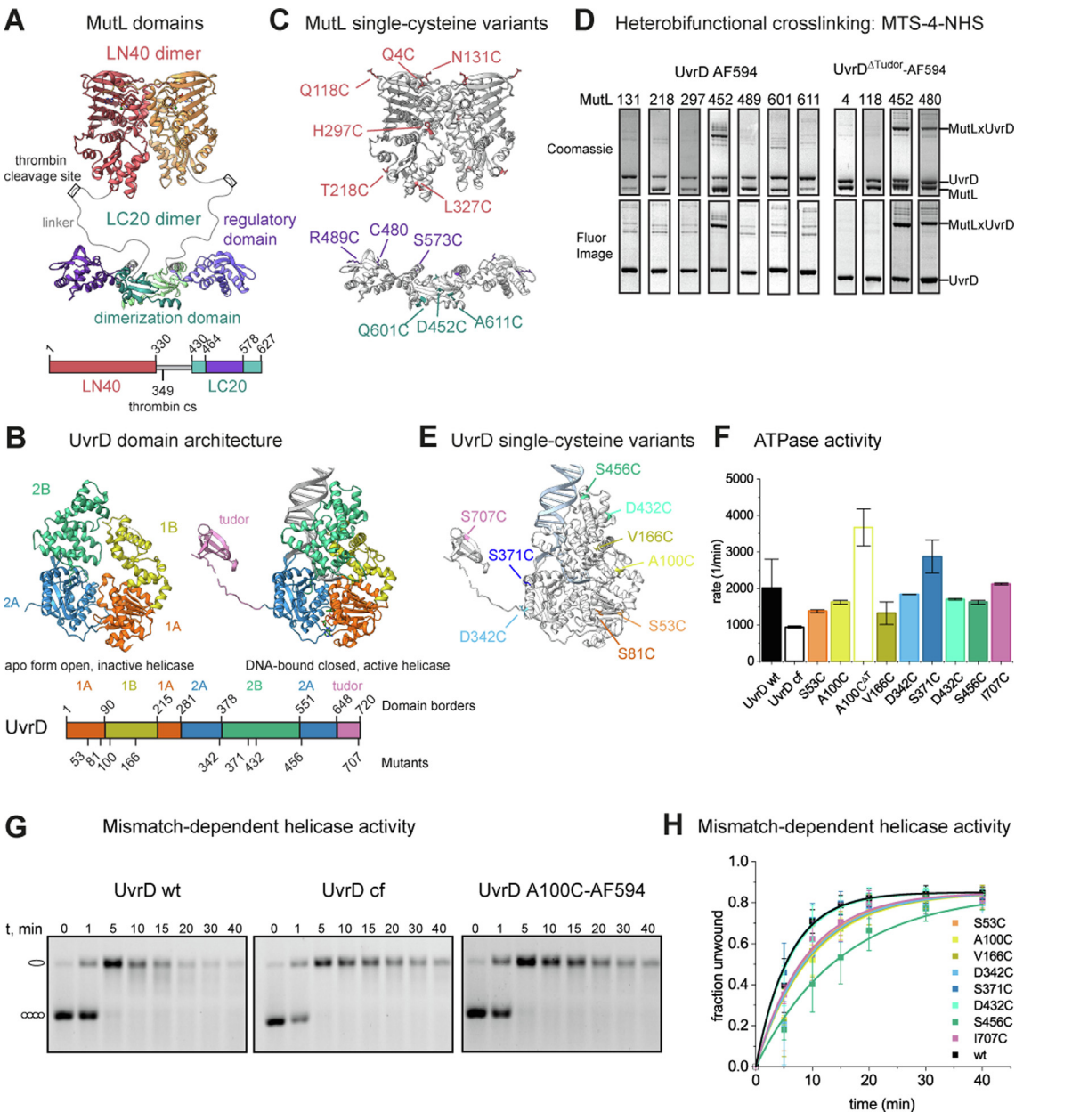

Figure 1. UvrD crosslinks to MutL C-terminal domain. (A) Domain architecture of the MutL dimer. The MutL C-terminal domains $MutL^{LC20}$ dimerize through the dimerization domains (shades of green) which are flanked by the regulatory domains (shades of purple) (pdb-id: 1x9z). The N-terminal domains $MutL^{LN40}$ in red and yellow dimerize upon ATP/AMPPNP addition (pdb-id: 1b63). A natural thrombin cleavage site is in the linker region, dividing MutL in LN40 and LC30 fragments. (**B**) Domain architecture of UvrD in apo form (pdb-id: 3lfu) on the left and DNA- and ADP MgF_3-bound (pdb-id: 2is6) on the right. Domains 1A in orange, 2A in blue and 1B in yellow remain most of their conformations while 2B in green switches between an open and a closed conformation of the helicase. The Tudor domain (AlphaFold prediction) at the very C-terminus of UvrD is connected through a flexible linker. (**C**) Single-cysteine variants of MutL used in this study (**D**) Heterobifunctional crosslinking between single-cysteine variants of MutL and lysines of UvrD or $UvrD^{\Delta Tudor}$. Top panel shows Coomassie-stained gel and bottom panel fluorescent-stained gels (gels adapted to align equivalent bands). Full gel images are in Supplementary Figure 1**C** (**E**) Single-cysteine variants of UvrD generated and characterized in this study. (**F**) ATPase activity of UvrD single-cysteine variants (mean and standard deviations (SD) for $n = 2$ experiments). (**G**) Time course of 40 min monitoring MutS-dependent nicking (conversion of supercoiled species on the gel into open circle) and unwinding and excision (disappearance of the nicked species) of a circular dsDNA substrate containing a G/T mismatch and single hemimethylated GATC site. Shown are example gels of UvrD WT (left), cysteine-free UvrD (middle) and UvrD A100C labelled with AF594 (right). All other gels can be found in **Supplementary** Figure 1**D**. (**H**) Quantification of the band intensities (mean and SD for $n = 2$–4 experiments) for all UvrD variants and global fit with a single exponential function (see Supplementary Table 1).

combination of MutL D452C and UvrD S456C resulted in the highest activity of crosslinked species. Interestingly, we discovered that once the two proteins are crosslinked, the N-terminal part of MutL can be removed without diminishing the stimulating effect on UvrD. This highlights the essential role of the C-terminal domain of MutL in facilitating the helicase activity of UvrD, as it is both required and sufficient for stimulation on DNA substrates with short 3′ ssDNA tails.

Results

UvrD crosslinks to MutL C-terminal domain

To gain insights into the interaction between UvrD and MutL, we conducted crosslinking experiments using the cysteine/lysine-specific crosslinker N-succinimidyloxycarbonylpropyl Methanethiosulfonate (MTS-4-NHS). We used previously characterized single-cysteine variants of MutL, distributed across the LN40 and LC20 domains,[28,33] to investigate the region of MutL involved in the interaction with UvrD (Figure 1C). These mutants were crosslinked to lysines in UvrD or UvrD lacking the Tudor domain ($UvrD^{\Delta Tudor}$) (Supplementary Figure 1A). For better visualization of the crosslinked species, we used the fluorescently labelled UvrD single-cysteine mutant A100C.[57] Crosslinking reactions involving the single-cysteine variants D452C and 480C, located in the $MutL^{LC20}$ region, showed prominent bands on Coomassie-stained SDS gels (Figure 1D, top panel) and fluorescent-imaged gels (Figure 1D, bottom panel) while all other MutL variants exhibited only a background pattern of non-specific crosslinks.

To refine our analysis and study the MutL-dependent helicase activation of UvrD, we generated single-cysteine variants of UvrD. Based on the previously characterized cysteine-free variant[54] we designed and produced nine mutants, distributed across all five domains of UvrD (Figure 1E). We validated the integrity and functionality of these mutants through various assays. Most of the variants exhibited ATPase activity comparable to that of the wild-type and the cysteine-free UvrD protein (Figure 1F), indicating proper folding and functionality. We compared the unwinding activity of these variants to UvrD WT, cysteine-free UvrD, and AF594-labeled UvrD A100C using our previously described unwinding assay.[23] The quantification of the fraction of unwound DNA showed similar or slightly reduced unwinding abilities for all the variants (Figure 1G–H, Supplementary Table 1, Supplementary Figure S1D), except for UvrD S456C, which displayed ~2-fold reduced activity. In conclusion, the generated single-cysteine variants of UvrD exhibited functional ATP hydrolysis and unwinding activities, making them suitable for further experiments. The results indicate that UvrD crosslinks and therefore binds to the MutL C-terminal domain.

Crosslinks between $UvrD^{2B}$ domain and $MutL^{LC20}$ result in highly active species

To refine the observed interaction between UvrD and the $MutL^{LC20}$ domain, we performed homobifunctional crosslinking using single-cysteine variants on MutL and UvrD. In addition to the three previously tested $MutL^{LC20}$ single-cysteine variants at positions 480, 489 and 452[28] we expanded our repertoire in this domain by an additional variant at position 573 (Figure 1C). We examined the crosslinking behavior of these four mutants with the newly generated UvrD single-cysteine mutants utilizing homobifunctional crosslinkers of various lengths. The crosslinkers were based on either irreversible maleimide (BMOE and $BM(PEG)_3$) or reversible sulfhydryl (MTS-4-MTS and MTS-17-MTS) chemistry. The former forms covalent bonds with high specificity and few side products, while the latter allows testing whether the unwinding activity is a result of the crosslinks by reverting the formed bond in the presence of a reducing agent.

Using BMOE, the highest crosslinking yield, with a single prominent band at 150 kDa, was obtained by combining the MutL D452C mutant, located in the dimerization domain, with the UvrD S456C variant on the 2B domain (Figure 2A) (see Supplementary Figure S2B–D for other crosslinkers). Similar results were observed for the UvrD $S456C^{\Delta Tudor}$ variant, indicating that the Tudor domain is non-essential for this interaction. Our results agree with previous findings by Ordabayev et al.,[56] which demonstrated the significance of the $UvrD^{2B}$ domain in MutL activation. Notably, their study showed that a chimeric UvrD variant, in which the 2B domain was replaced with the corresponding domain from the Rep helicase, was no longer activated by MutL. In this study we find that the $UvrD^{1B}$ domain crosslinked to the MutL regulatory domain via UvrD V166C and MutL 480C and R489C (Supplementary Figure S2A–D). The UvrD variant S707C, located in the Tudor domain, exhibited a high molecular weight band with the majority of MutL variants and crosslinker combinations. Crosslinks involving the Tudor domain display faster migration and appear at lower molecular weights.

To evaluate the functional relevance of the captured complexes, we conducted two assays to assess their unwinding activity. The first assay utilized a single-turnover approach with stopped-flow, as previously described.[47] The second assay was an adaptation of the first one for use in a plate reader, enabling the measurement of steady-state kinetics and facilitating higher throughput screening. As a proof of concept, we examined whether the single-cysteine variant of MutL (D452C) could activate UvrD (S456C) without the need for crosslinking. The assays were performed either in buffer T or buffer M20/20. Higher activities with UvrD and MutL-activated UvrD have been reported

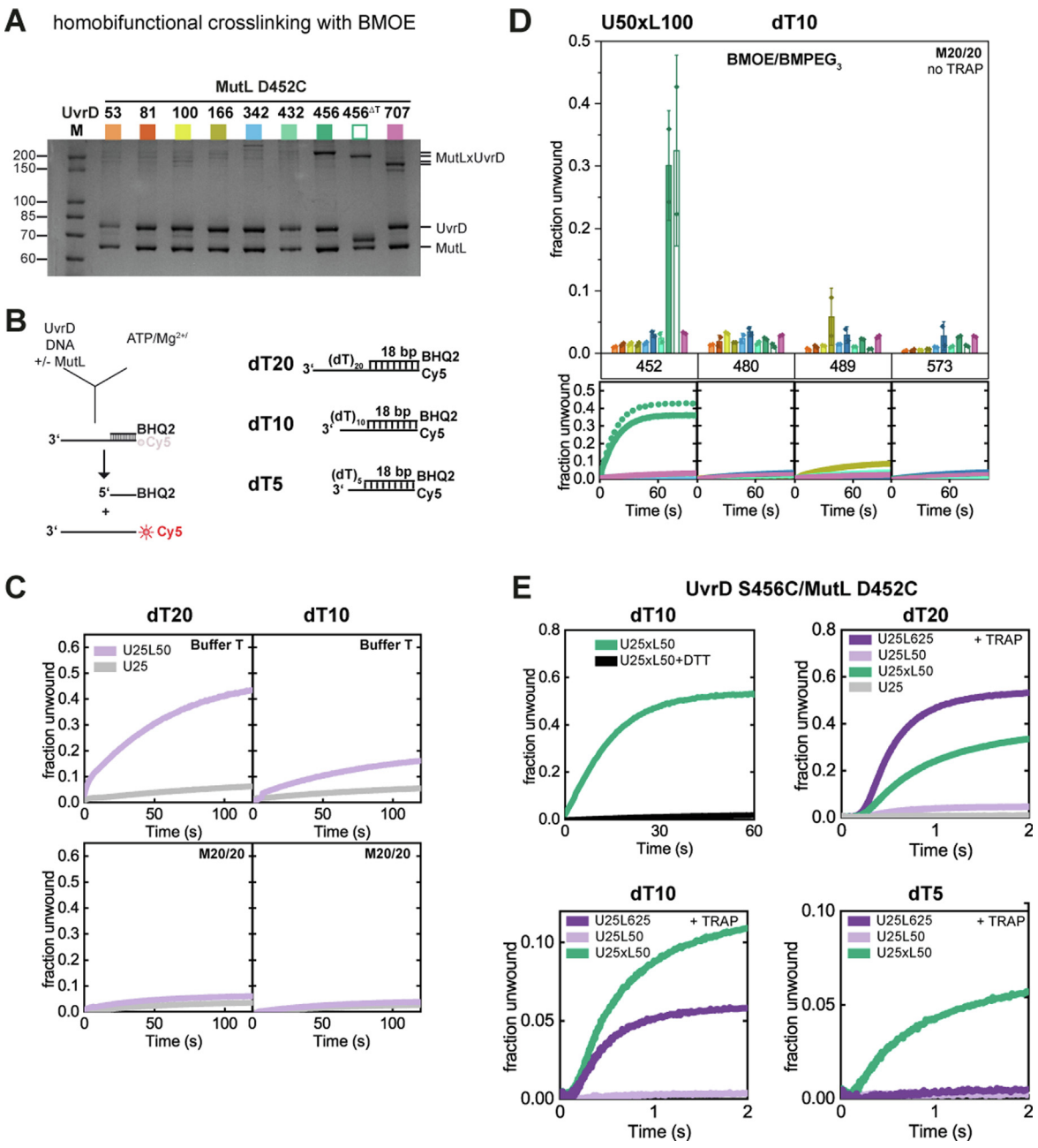

Figure 2. Crosslinks between UvrD^{2B} domain and MutL^{LC20} result in highly active species. **(A)** Homobifunctional crosslinking between MutL D452C and single cysteine-variants of UvrD using BMOE. Colors for UvrD are as indicated in Figure 1E (see Supplementary Figure 2 for S371C) (**B**) Schematics and substrates of the unwinding assays. (**C**) Steady-state unwinding assay in the plate reader with UvrD S456C alone (grey) or uncrosslinked MutL D452C and UvrD S456C (purple). Top panels in Buffer T, bottom panels in buffer M20/20. Left panels with dT_{20} substrate, right panels with dT_{10} substrate (**D**) Quantitative analysis of unwinding assay of BMOE or $BM(PEG)_3$ crosslinked species under multiple-turnover conditions (plate reader, UvrD 50 nM/MutL100 nM). MutL single-cysteine variant are indicated on X-axis. Colors of single-cysteine variant of UvrD as in **A** (dotted line for ΔTudor). Mean and SD for n = 2 experiments. (**E**) **Top Left:** Multiple-turnover unwinding assay of MutL D452C and UvrD S456C crosslinked with MTS-4-MTS, performed both without (green) and with DTT treatment to reverse the crosslink (black). **Top Right** and **Both Bottom Panels:** Single-turnover unwinding assays employing substrates featuring 3′-ss DNA tails of varying lengths (20, 10, 5 nt). Remarkably, a short 3′-ssDNA tail is sufficient for unwinding by the crosslinked MutL D452C and UvrD S456C complex (green). Controls include non-crosslinked proteins utilizing low MutL D452C concentration (light purple), high MutL D452C concentrations (dark purple), or the absence of MutL altogether (grey). Specific DNA substrate configurations are indicated above each corresponding box and in **B**.

in buffer T compared to buffer M20/20.[47] However, MutL exists as a mixture of dimers and higher oligomeric species in buffer T, whereas in buffer M20/20, the MutL dimer is stable[61] and forms a defined complex with UvrD and DNA in a 2:1:1 stoichiometry.[47]

The DNA substrates consisted of 18 bp duplex DNA flanked by a 3′ ssDNA tail with lengths of 5, 10 or 20 nt (short dT_5, dT_{10}, dT_{20}) (Figure 2B). Upon unwinding, the quenched Cy5 label at the end of the DNA duplex was released and this change in fluorescent signal was read out (Figure 2B). UvrD and MutL were preincubated with the DNA substrate, and the unwinding reaction was started upon ATP and Mg^{2+} addition. In the stopped-flow assay, a DNA hairpin trap prevented UvrD from rebinding the DNA substrate, creating single-turnover events.[47]

We then repeated this experiment using the plate reader system without DNA-trap and obtained similar results for the dT_{20} substrate (Figure 2C top left panel). As expected from Ordabayev et al.,[47] on a dT_{10} DNA substrate, MutL showed only mild stimulation of unwinding (Figure 2C top right panel). We then switched to a phosphate buffer (M20/20) to prevent MutL aggregation. As observed in Ordabayev et al., the unwinding signal was relatively weak under these conditions for both dT_{10} and dT_{20} DNA substrate[47] but sufficient for analysis.

With these proof of concepts at hand, we began assessing whether our crosslinking captured relevant species. We analyzed the crosslinked complexes for their ability to unwind DNA substrates using the plate reader assay. We measured samples of the MutL-UvrD crosslinking reactions with all four crosslinkers. The result of the more specific crosslinkers BMOE and BM $(PEG)_3$ were similar, and their combined data are shown in Figure 2D. Substantial unwinding was observed for the combination of MutL D452C and UvrD S456C. This high activity correlates well with the significant amount of crosslinked complex observed (Figure 2A). Some activity is also seen for MutL R489C and UvrD V166C in accordance with a specific complex band visible on the SDS gel. On the other hand, the crosslinked species that were observed for MutL D452C and UvrD S707C (Tudor domain) (Figure 2A last lane) did not show any unwinding activity (Figure 2D). The Tudor domain is tethered through a flexible linker to the core of UvrD, which allows crosslinking, but this covalent bond does not enable the activation of UvrD unwinding.

In addition, we tested the complexes crosslinked with the more reactive MTS-4-MTS or MTS-17-MTS crosslinkers (Supplementary Figure 2E). Interestingly, although for MTS-17-MTS there are several crosslinking combinations (Supplementary Figure 2E right panel) only some showed higher unwinding rates. Consequently, only some of the crosslinked bands capture relevant complexes. Given the length of this crosslinker of 24.7 Å[62] it seems likely that the effect we see is due to proximity rather than a trapped conformation.

Subsequently, we proceeded to validate the most promising complex of MutL D452C and UvrD S456C in the stopped-flow assay by reversing the crosslinking. We crosslinked the variants using MTS-4-MTS crosslinker and tested for unwinding of a dT_{10} substrate (Figure 2E top left panel). Addition of the reducing agent DTT to reverse the crosslink between MutL and UvrD, results in strongly reduced unwinding efficiencies similar to those with non-crosslinked MutL and UvrD (Figure 2E top left panel and Figure 2C bottom right panel). We concluded that the increased unwinding activity can be attributed to the crosslinking.

Previous research determined that a 3′ ssDNA tail of at least 10 nt was necessary for MutL activation of UvrD in non-crosslinked complexes suggesting an interaction of MutL with the 3′ ssDNA tail.[47] We revisited this question in the context of the UvrD-MutL crosslinked complex. As observed in published results, higher MutL D452C concentrations led to increased UvrD S456C helicase stimulation on a dT_{20} substrate in Buffer M20/20 (Figure 2E, top right panel), but with shorter 3′ ssDNA tails (10 or 5 nt) activation by MutL was less. (Figure 2E, bottom panel). However, when UvrD was crosslinked to MutL, we found that a 3′ ssDNA tail as short as 5 nt was sufficient to activate UvrD helicase (Figure 2E). As UvrD also needs at least 4 nt for binding,[46] this suggests that once MutL is crosslinked to UvrD, the 3′ ssDNA tail is not further required for activation.

MutL and UvrD crosslink into an active 2:1 stoichiometric complex

Adequate crosslinking yields were achieved with MutL D452C and UvrD S456C, although the reaction still contained uncrosslinked MutL and UvrD, as well as other crosslink products. To optimize the reaction, we assessed the influence of DNA (using dT_{20} DNA substrate) and AMPPNP on crosslink yield and specificity (Figure 3A), and found that crosslinking improved when both components were included, albeit not quantitatively. A further enhancement in MutL-UvrD crosslinking was achieved by using a phosphate buffer containing potassium instead of sodium (Figure 3B, a quantitative analysis of crosslinking yields using the MTS-4-MTS crosslinker is shown in the Supplementary Table 2). We employed size-exclusion chromatography to purify the MutL-UvrD crosslink complex, separate uncrosslinked UvrD from crosslinked MutL-UvrD, and determined the complex's stoichiometry (Figure 3C). The elution profile displayed two main peaks (≈10.5 ml and 14.5 ml). Notably, only the first peak contained the MutL-UvrD crosslink and uncrosslinked MutL (as shown by SDS-PAGE analysis), with no visible

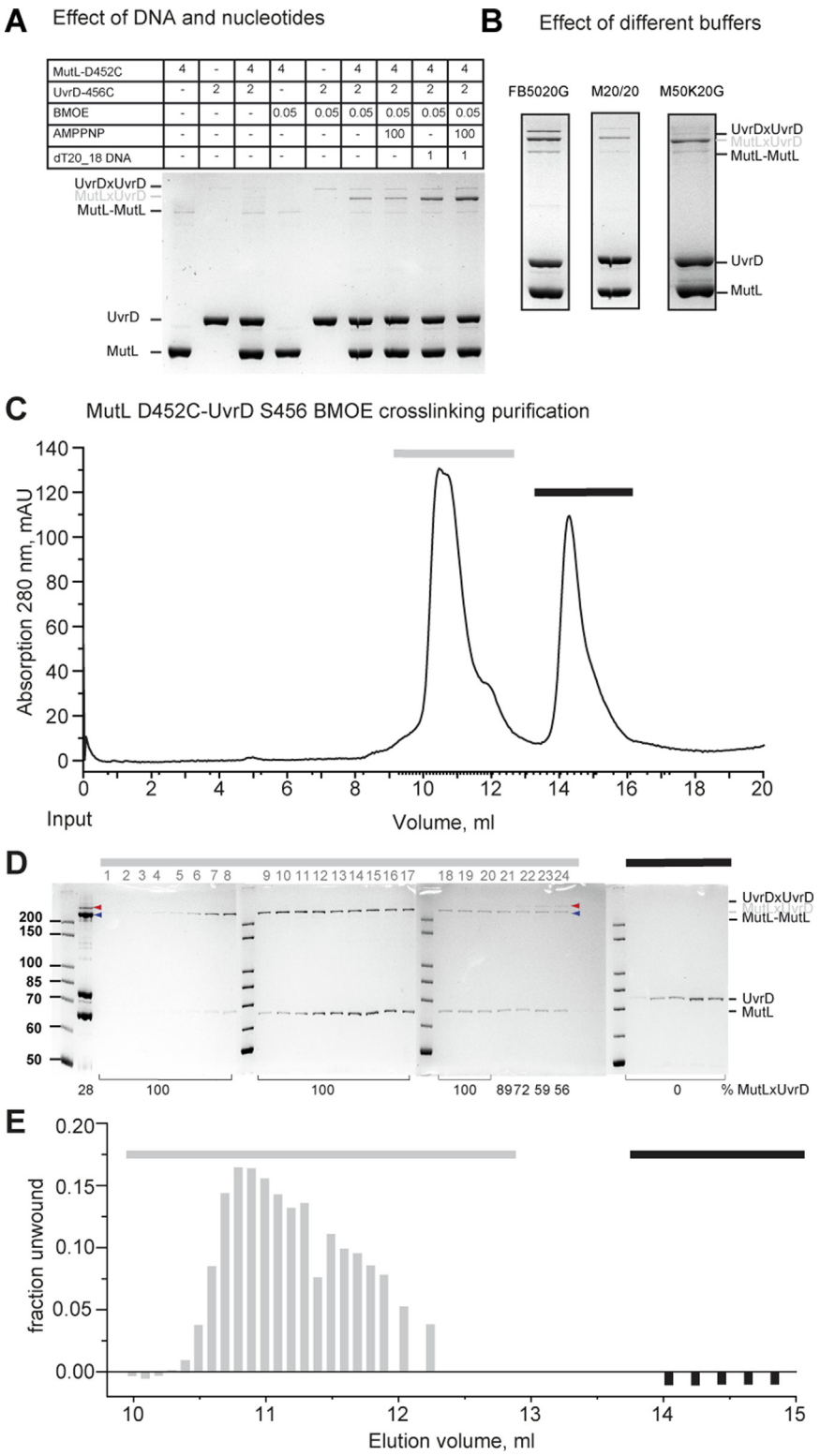

Figure 3. MutL and UvrD crosslink into an active 2:1 stoichiometric complex. (**A**–**B**) Optimization of crosslinking efficiency. (**A**) The MutL-UvrD yield increased upon DNA substrate and nucleotide addition in Buffer M20/20. (**B**) Effect of different buffers on crosslinking yield and formation of side-products (UvrDxUvrD or MutLxMutL) (**C**) Size exclusion chromatography elution profile of MutL D452C (20 μM) crosslinked with UvrD S456C (10 μM) with BMOE (0.12 mM) in buffer M100K20G, (**D**) corresponding SDS-PAGE analysis of indicated fraction (grey and black bar) (**E**) and multiple-turnover unwinding assay using the 3′-$(dT)_{10}$ tailed DNA substrate.

bands for UvrD (Figure 3D). This peak likely represents a complex composed of a MutL dimer with one subunit crosslinked to a UvrD monomer, in line with stoichiometry from prior experiments.[47] The second peak only contained a single major band corresponding to uncrosslinked UvrD. Subsequently, fractions were analyzed for DNA unwinding activity under multiple-turnover conditions. As expected, only fractions containing the crosslinked MutL-UvrD complex demonstrated DNA unwinding activity (Figure 3E. The specific activity, i.e. [nM DNA unwound]/[nM UvrD] increased from 0.18 for the input to 0.41 ± 0.05 for fractions 9–14.

In conclusion, these results support the notion that the formation of crosslinks between MutL and UvrD promotes the observed DNA unwinding activity at low concentrations.

MutL C-terminal domain alone can activate UvrD unwinding

Our investigations so far have demonstrated that UvrD helicase activation can be achieved by crosslinking single-cysteine residues in the C-terminal LC20 domain of MutL to UvrD 2B and 1B domains, resulting in a highly active DNA unwinding complex. To delve deeper into the role of the N-terminal LN40 domain of MutL in this activation, we exploited the intrinsic thrombin cleavage site located near the LN40 domain in the linker region of MutL.[26] Thrombin cleavage effectively removed LN40 (residues 1–349), allowing us to evaluate the isolated effect of the LC30 domain (residues 350–615).

After crosslinking MutL D452C to UvrD S456C with MTS-4-MTS, we achieved complete cleavage of MutL into LN40 and LC30 by thrombin (Figure 4A lane 5 + 7). As a control, we also reversed the crosslinking reaction with DTT treatment (Figure 4A lane 6 + 8). We then assessed the DNA unwinding activity of both uncrosslinked (MutL 625 nM or 50 nM, UvrD 25 nM) and crosslinked (MutL 50 nM, UvrD 25 nM) samples before and after thrombin cleavage under single-turnover conditions. As anticipated from previous studies,[26] the ability of MutL to activate UvrD was completely lost upon thrombin cleavage (Figure 4B dotted purple line). In contrast, the thrombin-cleaved crosslinked complex exhibited only a minor decrease in DNA unwinding activity compared to the uncleaved crosslinked complex (Figure 4B dotted green and solid green lines, respectively). This observation held true also under multiple-turnover conditions and for DNA substrates with a shorter 3′-ssDNA tails (Figure 4B right panel). We concluded that the stimulation of UvrD DNA unwinding activity can be achieved by the C-terminal domain of MutL alone, but only when covalently linked to UvrD.

To rule out the effect of the LN40 fragment on DNA unwinding reaction in the previous experiment, we purified the MutL^{LC30} D452C fragment, obtained by thrombin cleavage of MutL D452C, using gel filtration. We then tested whether crosslinking between MutL^{LC30} D452C to UvrD (UvrD S456C or UvrD$^{\Delta Tudor}$ S456C) using BMOE is possible. Indeed, the C-terminal fragment of MutL formed a covalent complex with both UvrD variants (Figure 4C lane 5* and 7*). Moreover, only the crosslinked samples demonstrated DNA unwinding activity using the dT_{10} DNA substrate (Figure 4D dark and light green), while the uncrosslinked proteins showed no detectable DNA unwinding activity (Figure 4D light magenta).

In summary, our findings suggest that while the LN40 domain, which can bind to DNA likely contributes to DNA binding and thereby complex formation between MutL, UvrD and DNA for optimal interaction, it seems not essential for the stimulation of DNA unwinding. On the other hand, the LC30 domain alone, which is not able to bind to DNA on its own[26], is not only sufficient for interaction with UvrD[17] (Figure 4C) but, when crosslinked to the UvrD 2B domain, it is fully capable of activating the UvrD helicase.

Discussion

In this study, our primary objective was to explore the mechanism by which MutL stimulates the UvrD DNA unwinding activity, thereby gaining insight into the functional significance of the MutL-UvrD interaction in DNA mismatch repair. We performed a series of site-specific crosslinking experiments using single-cysteine variants of MutL and UvrD (Figures 1D, 2A and Supplementary Figure 1C +2A–D) to investigate which variants forms covalent complexes. Interestingly, the formation of a crosslink did not necessarily correlate with stimulation of DNA unwinding. Several combinations of UvrD and MutL variants could be crosslinked with the longer MTS-17-MTS crosslinker, but only a few of these displayed increased helicase activity. For example, MutL D452C with UvrD S456C and MutL R489C with UvrD V166C showed increased activation, whereas the alternate combinations did not (Supplementary Figure 2F).

By combining these crosslinking experiments with functional unwinding assays, we were able to establish the importance of an interaction between MutL^{LC20} and the UvrD 2B domain in enhancing the DNA unwinding activity (Figure 2D + E and Supplementary Figure 2E). This is in agreement with previous analysis showing that a specific interaction between MutL and the UvrD 2B domain is required for helicase activation, while a UvrD chimera with the Rep^{2B} domain could not be activated by MutL.[56] In addition to the prominent MutL D452C UvrD S456C crosslink, which connected the dimerization domain of MutL and the 2B domain of UvrD, we also observed another

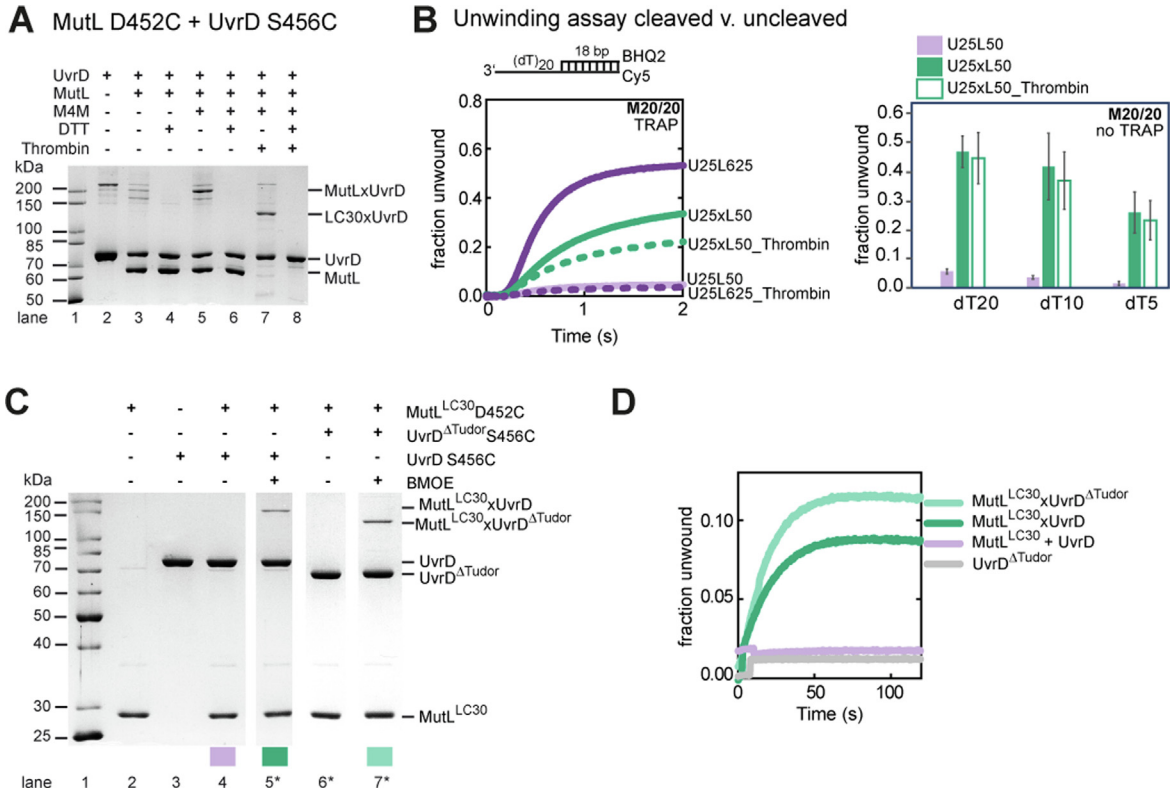

Figure 4. Activation of UvrD helicase by the MutL C-terminal domain. (**A**) SDS-PAGE analysis of MutL D452C and UvrD S456C crosslinked with MTS-4-MTS, both without and with thrombin or DTT treatment. (**B**) Single (left) and multiple-turnover (right) DNA unwinding reactions using MutL/UvrD either uncrosslinked (MutL/UvrD stoichiometry 25:1, dark purple or 2:1 light purple) or crosslinked with MTS-4-MTS (MutL/UvrD stoichiometry 2:1, green). The samples subjected to thrombin treatment are indicated by the dotted lines (left) or unfilled bars (right), respectively. Mean and SD for $n = 2$ experiments. (**C**) Crosslinking of the MutL D452C^{LC30} fragment with UvrD S456C or UvrD$^{\Delta Tudor}$ S456C using BMOE. (**D**) Multiple-turnover DNA unwinding reaction using a dT_{10} substrate with UvrD$^{\Delta Tudor}$ S456C alone (gray), uncrosslinked (light purple) and crosslinked complexes of MutL D452C^{LC30} and UvrD S456C (dark green) or UvrD$^{\Delta Tudor}$ S456C (light green), respectively corresponding to experiments shown in **C**.

intriguing crosslink between MutL R489C (located in the regulatory domain) and UvrD V166C (situated in the 1B domain). This crosslinked complex, formed using the longer-range MTS-17-MTS crosslinker, resulted in a significant enhancement of helicase activity (Supplementary Figure 2E). This observation suggests a potential interaction between the regulatory domain of MutL and the 1B domain of UvrD, which may play a role in stimulating UvrD's helicase activity. Based on our data, we propose that MutL and UvrD facilitate active unwinding through the proximity of MutL's dimerization and regulatory domains with UvrD's 2B and 1B domains, respectively.

These results are in line with a model suggestion that the MutL-UvrD complex exist in more than one conformation (similar as UvrD) that are not all active.[56] It has been observed in single-molecule FRET experiments that UvrD (labeled at the 1B and 2B domain) in complex with DNA and MutL exists in at least three distinct conformations (open, intermediate, closed) as judged by FRET efficiencies as a measure for conformation and distance between the 1B and 2B domain.[56] The absence of activity even when a crosslink was formed could be trapping the complex in one of the inactive conformations of UvrD.

Previous yeast two-hybrid studies showed that for physical interaction with UvrD the C-terminal fragment (residues 398–615) of MutL was sufficient,[17] however, for helicase activation the integrity of the MutL protein was critical.[26] Moreover, systematic studies on the 3′ ssDNA tail length suggested that MutL likely interacts with part of the 3′ ssDNA tail during UvrD binding and activation UvrD.[47] We discovered that upon crosslinking of MutL and UvrD the requirement for an extended 3′ ssDNA tail was abolished (Figure 2E), suggesting that once the complex is stabilized by a covalent bond, the interaction between MutL and the 3′ ssDNA tail is no longer required. This is in line with our observation that enzymatic removal of the N-terminal LN40 part of MutL, which contain the DNA binding activity of MutL,[30,63] from the cross-

linked complex or crosslinking only MutL^{LC30} to UvrD (through MutL D452C and UvrD S456C) (Figure 4A + C and Supplementary Figure 4) retained an active unwinding complex (Figure 4B), suggesting that the LN40 is not essential for the DNA unwinding simulation. Interestingly, in contrast to experiments with the *E. coli* proteins, the C-terminal domain (residues 303–425) of the MutL orthologue from *Aquifex aeolicus* was sufficient to activate UvrD, albeit at a reduced efficacy compared to full-length MutL.[64]

To gain insights into the structural details of the MutL-UvrD interaction, we initially attempted to model the interaction with Haddock.[65,66] The docking provided numerous potential options, but the high degree of variability between the proposed interactions, as well as the MutL dimer made confident predictions challenging. We then used AlphaFold multimer[67] within the ColabFold platform[68] on the full-length proteins. Structures of individual domains in this prediction are in accordance with crystal structures. A measure of confidence in the global relative positioning of groups of residues in space can be read out in the PAE matrix[69] (Supplementary Figure 5A). Although the positioning of MutL^{LN40} onto UvrD could be of value, we focus here on the interaction between UvrD and the MutL^{LC20} domain. Repeat predictions yielded one preferred solution for the positioning of MutL^{LC20} relative to the UvrD^{2B} domain, with distances between residues 452 in MutL and 456 in UvrD consistent with our crosslinking data. (Supplementary Figure 5B), although confidence in this prediction was not very high, as seen by the shading of green in the PAE matrix between MutL^{LC20} and UvrD^{2B}. The two MutL^{LC20} domains form the expected dimer[28] and as a consequence result in a somewhat less confident prediction for the more distant MutL^{LC20} in relation to UvrD^{2B}. All in all, the fact that the relative position of one MutL^{LC20} and UvrD^{2B} was repeatedly found in predictions in which MutL is varied (dimer, monomer, LC20 domain alone) does support its likelihood.

Interestingly, in these repeats, the orientation of the 2B domain within UvrD varies between its position observed in the apo UvrD structure and that observed in the DNA complex, and the MutL^{LC20} moves with it. In fact, AlphaFold has little confidence in the placement of UvrD^{2B} relative to the rest of UvrD, as seen from the PAE matrix (Supplementary Figure 5A). While the apo-state would be incompatible with DNA binding and helicase activity, it is plausible that the uncertainty in the positioning of the UvrD^{2B} domain reflects an intermediate state adopted by UvrD or high flexibility of the 2B domain when bound to MutL, as suggested by data from the Lohman group.[56]

Given these uncertainties and the flexibility of both UvrD and MutL, we cannot at this stage provide a detailed model of how MutL activates UvrD. It is tempting to speculate the simultaneous interaction between the MutL regulatory and the dimerization domain with the 1B and 2B domains of UvrD could reduce the conformation flexibility of UvrD in favor of the intermediate and closed conformation (and hence preventing the open conformation that is incompatible with DNA unwinding).

In summary, our present study has provided valuable and innovative insights into the physical and functional interaction between MutL and UvrD. It underscores the significance of the MutL C-terminal domain's interaction with the UvrD 2B and 1B domains. Additionally, our approach of combining complex trapping states with functional analysis has proven to be crucial in dissecting the multiple dynamic states of these complexes, particularly considering the inherent flexibility of the UvrD^{2B} domain, which can adopt several intermediate states between open and closed conformations.[56] To gain a more comprehensive understanding of the molecular intricacies and dynamics involved in MutL's activation of UvrD, future studies that integrate the crosslinking approach with other structural or biophysical methods such as crystallography, cryo-EM, single-molecule FRET, or mass spectrometry will be indispensable. Furthermore, as MutS-dependent recruitment of MutL to DNA requires the LN40 domains, and unwinding initiates from a nick, it will be interesting to place the findings of this work in the context of the full MMR system.

Material and Methods

Buffers

Buffers were prepared with reagent grade chemicals using distilled water that was deionized using a Milli-Q water purification system (Millipore Corp., Bedford, MA). Buffers, used for purification: UvrD-binding buffer: 20 mM Tris–HCl (pH 7.5), 500 mM NaCl, 10 mM imidazole, 1 mM DTT, 1 mM PMSF, 20% (v/v) glycerol; UvrD Ni-washing buffer: 20 mM Tris–HCl (pH 7.5), 500 mM NaCl, 25 mM imidazole, 1 mM DTT, 1 mM PMSF, 20% (v/v) glycerol; UvrD Ni-elution buffer: 20 mM Tris–HCl (pH 7.5), 500 mM NaCl, 1 mM PMSF, 40–200 mM imidazole, UvrD dialysis buffer: 20 mM Tris–HCl (pH 8.3), 300 mM NaCl, 1 mM EDTA, 2 mM DTT, 20% (v/v) glycerol. Buffer A: 20 mM Tris–HCl (pH8.3), 100 mM NaCl, 1 mM EDTA, 20% (v/v) glycerol; buffer B: 20 mM Tris–HCl (pH8.3), 1 mM EDTA, 20% (v/v) glycerol; UvrD storage buffer: 25 mM HEPES (pH 8.0), 400 mM KCl, 20% (v/v) glycerol. MutL lysis buffer:20 mM Tris–HCl (pH 8.0), 1 M NaCl, 5 mM imidazole, 1 mM PMSF, 10% (v/v) glycerol, MutL wash buffer: 20 mM Tris–HCl (pH 8.0), 1 M NaCl, 10 mM imidazole, 1 mM PMSF, 10% (v/v) glycerol, MutL elution buffer: 20 mM Tris–HCl (pH 8.0), 1 M NaCl, 500 mM imidazole, 1 mM PMSF, 10% (v/v) glycerol, MutL HPLC and storage buffer

10 mM HEPES-KOH (pH 8.0), 1 mM EDTA, 500 mM KCl, 10% (v/v) glycerol.

Buffers used for activity assays: Buffer T20[70] is 10 mM Tris–HCl (pH 8.3 at 25 °C), 20 mM NaCl, and 20% (v/v) glycerol, Buffer M20/20: 40.5 mM K_2HPO_4, 9.5 mM KH_2PO_4, 20 mM NaCl, 20% (v/v) glycerol, mismatch-dependent helicase buffer FB150T10G: 25 mM HEPES-KOH (pH 7.5) 150 mM KCl, 5 mM MgCl2, 0.005% (v/v) Tween 20, 100 ng/μl BSA, 1 mM DTT10% (v/v) glycerol.

Buffers used for cross-linking: Buffer FB50T 20G: 25 mM HEPES pH 7.5, 50 mM KCl, 0.005% (v/v) Tween 20, 5 mM $MgCl_2$, 20% (v/v) glycerol, buffer M/M: 40.5 mM K_2HPO_4. 9.5 mM KH_2PO_4, 50 mM KCl, 5 mM $MgCl_2$; buffer M50K20G: 40.5 mM K_2HPO_4. 9.5 mmKH_2PO_4, 50 mM KCl, 5 mM $MgCl_2$, 20% (v/v) glycerol; buffer M100K10G has the same composition but with 100 mM KCl (pH 7.4 at 25 °C) and 10% (v/v) glycerol. ATP, ATPγS and AMPPNP were purchased from Jena Bioscience.

Expression constructs and mutagenesis

pA10 UvrDΔCys and pA10 UvrDΔCys[A100C] plasmids[54] were a kind gift form Timothy M. Lohman. In the pA10 UvrDΔCys plasmid, the six native cysteine residues (C52, C181, C322, C350, C441, and C640) of UvrD were replaced with serine residues. The pA10 UvrDΔCys[A100C] plasmid contains a single cysteine at position 100. In addition, both plasmids have a hexahistidine (6xHis) tag and a thrombin cleavage site (MGSSHHHHHHSSGLVPRGSH, 20 aa) fused to the N-terminus of UvrD.

For the crosslinking and labelling experiments, eight different single-cysteines were cloned into the pA10 plasmid. The selection process for the newly introduced residues was driven by the following criteria: (i) non-conserved (ConSurf)[71], (ii) surface-exposed, accessible (SDM)[72], and (iii) does not reduce UvrD stability (iStable).[73] The following variants were selected and introduced by site-directed mutagenesis using NEB GibsonAssembly kit: S53, S81, A100, V166, D342, S371, D432, D456, I707.

Furthermore, to bypass using thrombin and having the risk of cleavage at noncanonical sites, a TEV-cleavage side was inserted additionally before the UvrD coding sequence. Briefly, pET15b was cleaved with BamHI and NdeI restriction enzymes to create the vector backbone. UvrD sequence was amplified from pA10 UvrDΔCys vector with primers containing the TEV cleavage site (pf716 + pf717 for the full-length and pf716 + pf721 for UvrDΔ73). pA10 UvrDΔCys, pA10 UvrDΔCys[A100C], pET9D UvrDwt were used as templates for the PCR amplification. All except of A100C single Cys variants were generated according to the NEB Gibson Assembly protocol by combining 2 PCR fragments obtained by amplification of pA10 UvrDΔCys with pf716 + reverse primer of each variant and forward primer + pf717. All primers are listed in the Supplementary Table 3. For MutL variants D452C, 480C and R489C a TEV-cleavage site was introduced at the N-terminus of MutL in pTX418 MutL[ΔCys],[28] similar to UvrD (primers pf738 + pf739). All mutations were confirmed by colony PCR and verified by DNA sequencing.

Protein expression and purification

Wild type MutS, MutL and MutH were expressed and purified as described.[74,75] For the purification of MutL constructs containing the TEV-cleavage site, an additional cleavage step was introduced during dialysis with subsequent removal of uncleaved protein using a Ni-NTA column. UvrD was purified using pET15b-UvrD as described[76] with a slight modification: His-tagged UvrD was overexpressed in BL21 StarTM(DE3)pLysS cells in the vector pET15b and purified using a Protino Ni-IDA 2000 column (Macherey Nagel). The N-terminal His6-tag was cleaved by TEV protease in dialysis buffer over night at 4 °C. The cleaved protein was passed through Ni-NTA (Qiagen) to remove uncleaved protein, His-tag, and His-tagged TEV-protease, followed by Heparin, HiTrapQ, and lastly buffer exchange into UvrD storage buffer using ZebaSpin desalting columns (40 K MWCO, ThermoFisher Scientific). All purified proteins were flash-frozen in liquid nitrogen and stored at −80 °C. Concentrations were determined spectrophotometrically by using the theoretical extinction coefficients. Single-stranded DNA-binding protein (SSB) was purchased from Promega (Madison, USA) and exonuclease I (ExoI) from New England Biolabs (Ipswich, USA).

DNA oligonucleotides and substrates

All primers for UvrD and MutL mutagenesis (HPLC grade) were synthesized by Biolegio (Nijmegen, Netherlands), all other oligonucleotides were synthesized by Eurogentec (Seraing, Belgium). For the DNA unwinding substrate with 18 bp duplex and 3´-flanking dT(x)tail, two complementary oligonucleotides were diluted in annealing buffer (10 mM Tris–HCl (pH 8.0) and 50 mM NaCl). As a result of mixing two oligonucleotides, the final concentration of the duplex was 20 μM. The UvrD dT_{40} hairpin Trap was annealed at the concentration of 50 μM. Duplex DNA was formed by annealing at 95 °C for 5 min followed by a gradient decrease in temperature by 5 °C every five minutes.

Hemimethylated DNA substrate containing a single G/T mismatch was generated and purified as described[23] using primer GT28 (5′-GGT AGC TCT TCA-T*-CC GCA AAC AAA CC-g-CCG CTG GTA GCG-3′), where the g indicates the nucleotide forming the G/T mismatch, and the T* is the labelled nucleotide with Alexa Fluor ® 647 (Alexa^{647}(IBA

GmbH, Göttingen, Germany). As a result of primer extension on ssDNA phagemid GATC1 (derivative of pGEM13Zf),[23] GT#1b^{647} was obtained, containing a GT mismatch at position 2215, and one hemimethylated GATC site which is 61 bp 3′ from the mismatch, and the fluorophore located close to the mismatch for quantitation. Closed circular hemimethylated DNA-substrate was gel-purified using a Promega gel purification kit.

ATPase assay

The ATPase activity of UvrD was determined using an NADH-coupled assay,[77] which measures the loss of NADH absorbance at 340 nm (ε = 625 0 cm^{-1} M^{-1}) due to the conversion of ADP back to ATP by pyruvate kinase and lactate dehydrogenase in the presence of phosphoenolpyruvate. Reactions (100 μL) were carried out in 96-well plate at room temperature using microplate absorbance reader (SUNRISE, TECAN) in buffer FB150T10G containing 0.4 mM NADH, 1% (v/v) enzyme mix (pyruvate kinase and lactate dehydrogenase; Sigma Life Sciences) 1 mM phosphoenolpyruvate (Sigma-Aldrich), 1 μM ssDNA (pF319), 0.1 μM UvrD and 1 mM ATP, which was added last to start the reactions. Extinction at 340 nm was recorded for 10 min, and the initial slope from the extinction vs. time plot was converted into (μM ATP hydrolysed)/(0.1 μM UvrD min) using a calibration curve obtained with ADP instead of ATP.

MutS-dependent unwinding of a circular substrate

MutS-dependent unwinding was performed similarly as described.[23] Nicking with subsequent DNA unwinding and excision of 0.5 nM GT#1b^{647} was monitored in the presence of 20 nM MutS, 20 nM MutL, 10 nM MutH, 20 nM UvrD, 200 nM SSB, 0.1 units of exonuclease I in FB150T10G reaction buffer containing 1 mM ATP. Reactions (25 °C) were started by combining equal volumes of a pre-assembled mixture of DNA with ATP in reaction buffer FB150T10G with a pre-assembled mixture of proteins. At selected time points, 10 μl aliquots were mixed with an equal volume of stop buffer (20% (v/v) glycerol, 1% (w/v) SDS and 50 mM EDTA) and electrophoresed over night at 20 V on a 0.8% (w/v) agarose gel in TAE buffer in the presence of 40 μM chloroquine. Incision and excision reaction products were visualized using a Typhoon FLA imager (Cytiva). The fluorophore was excited at 633 nm and its emission was passed through the Cy5 670BP30 filter. Band intensities were quantified using FIJI[78]. The fraction of unwound DNA substrate was calculated from the total fluorescent signal of the supercoiled and open circular species relative to that at time = 0 min for each reaction (see Supplementary Table 1 for details).

Heterobifunctional crosslinking using MTS-4-NHS

For heterobifunctional crosslinking, MutL single-cysteine variants (4 μM) were combined with UvrD (2 μM) labelled with AF594 at position A100C. Briefly, UvrD was purified as described earlier and incubated with 5 mM DTT. After 30 min on ice, the reducing agent was removed with the help of ZebaSpin desalting columns. Alexa Fluor®594 (Invitrogen) fluorescent dyes were diluted in DMSO, added in 3x molar access over the protein concentration and incubated in UvrD buffer B on ice for 2 h. Afterwards excess of dye was removed with ZebaSpin desalting columns and absorbance spectroscopy was used to determine the protein concentration and the degree of labelling (DOL). For UvrD DOL was >90%.

The crosslinking reaction was performed in 20 μl buffer FB50T20G (supplemented with DNA and/or AMPPNP when indicated). Proteins were incubated together for 3 min and the crosslinking reaction was started by addition of 200 μM MTS-4-NHS (Toronto Research Chemicals). After 5 min the reaction was stopped by adding 100 mM Tris–HCl, 7.5 mM N-ethylmaleimide and 5x SDS loading buffer. Samples were boiled for 2 min at 95 °C and half of the reaction was subjected to 8% SDS-PAGE at 200 V for 50 min. Imaging was performed for 100 ms first by Intas Chemostar ECL and Fluorescence Imager with EPI Fluorescence Light Cubes: LED Cube BLUE 477 nm for AF488 dye and LED Cube GREEN 535 nm for AF594-labeled proteins and then by Coomassie staining.

Site-specific cysteine crosslinking

ZebaSpin desalting columns were used to change storage buffer of protein samples to a buffer without reducing agent. UvrD at high concentrations does not tolerate low salt, therefore UvrD was buffer exchanged to 200 mM salt, while for the MutL sample the salt was reduced to 50 mM. Both protein samples were kept on ice. Initial crosslinking condition was in Buffer FB50 20G. The initial protocol was to combine 2 μM DNA, 2 μM UvrD, 4 μM MutL, 1 mM ATP in a tube, incubate for 5 min, followed by the addition of 400 μM crosslinker, incubate for 5 min, and finally stopping the reaction by adding 200 μM N-ethylmaleimide for the MTS-crosslinker and 1 mM DTT for maleimide crosslinker. Later, conditions were changed as indicated. Final crosslinking buffer: 50 mM K_2HPO_4/KH_2PO_4 pH 8.0, 100 mM KCl, 20% (v/v) glycerol. $MgCl_2$ was added together with ATP for the reaction, as $MgPO_4$ started precipitates over time at pH 8.0. Final concentration of crosslinker was 30 μM. Results were visualized on 8% SDS-PAGE.

MTS-4-MTS (1,4-Butanediyl Bismethanethiosulfonate) and MTS-17-MTS (MTS-17-O5-MTS, 3,6,9,12,15-Pentaoxaheptadecane-1,17-diyl Bis-methanethiosulfonate) were purchased from Toronto Research Chemicals, BMOE (bismaleimidoethane), $BM(PEG)_3$ (1,11-bismalei mido-triethyleneglycol) were obtained from ThermoFisher Scientific™.

Multiple-turnover DNA unwinding

18 bp DNA duplex with a BHQ2-quencher and a Cy5 fluorophore attached to the 3′ and 5′ end respectively, were formed by hybridization of top oligonucleotide 18_top_BHQ2_Orda with a bottom strand oligonucleotide (Cy5-UvrD(dT)x_18, where x corresponds to the length of the 3′ ssDNA tail, Supplementary Table 2).[47] Multiple-turnover DNA unwinding was measured in final volume of 200 μL in the indicated buffers in a TECAN infinite F200 fluorescence microplate reader using excitation filter (620 nm/ 10 nm) and emission filter (670 nm/25 nm) using a 50% mirror at 24–26 °C in 96-well plates (MICROPLATE, 96 WELL, PS, F-BOTTOM BLACK, NON-BINDING, Greiner bio-one). DNA (final concentration 125 nM) and proteins (UvrD, MutL or crosslinked samples thereof at the indicated concentrations) were preincubated in the indicated buffer for >5 min and the reaction was started by injection of 20 μL 10 mM ATP/20 mM $MgCl_2$ and fluorescence intensity was measured for 60–120 s. To obtain the maximum fluorescence values, nucleases (exonuclease I, exonuclease III and DNaseI) were added and the fluorescence was measured after 30 min. Fraction unwound was calculated from the buffer corrected signals normalized to the maximum fluorescence measured after exonuclease/DNase I treatment.

Single-turnover DNA unwinding

Single-turnover DNA unwinding kinetics were measured at 25 °C in Buffer T or M20/20 in a stopped-flow device SF-61SX2 (TgK Scientific, Bradford-on-Avon, UK) with a LED light source (LSM-635A LED Light Source, Ocean Insight) using excitation band pass prefilter filter (620 nm/10 nm). Emission was recorded with band pass filters (ET670/50 Chroma Technology, Olching, Germany) for the Cy5 fluorescence signal. Samples were mixed in 1:1 vol ratio in the indicated buffer, e.g. 125 nM DNA, 50 nM UvrD and 1250 nM MutL in syringe 1 were mixed with 1 mM ATP, 2 mM $MgCl_2$ and 20 μM of trap DNA (UvrD_trap_hairpin) given final concentrations of DNA 62.5 nM, UvrD 25 nM and MutL 625 nm indicated as U25L625 in the figure legends. Fraction unwound was calculated by normalization to the signals obtained with the single-strand Cy5-labelled bottom strand after correction for buffer background.

Gel filtration of MutL D452C-UvrD S456C crosslinked complex

For preparative crosslinking, MutL D452C and UvrD D456C variants were first incubated with 2 mM DTT for 1 h on ice. After that, the reducing agent was removed, and buffer was exchanged to the crosslinking buffer M100K10G using ZebaSpin columns. 20 μM MutL D452C was incubated with 10 μM UvrD456C for 5 min on ice in 800 μl reaction volume. After that, 3× access of BMOE (ThermoFisher Scientific) crosslinker was added, the reaction was mixed and incubated for 1 h on ice. The reaction was stopped with 2 mM DTT, proteins were centrifuged for 10 min at 4 °C to remove aggregates. The excess of unreacted reagent was removed from the crosslinking mixture by using ZebaSpin desalting columns, equilibrated with MutL-UvrD gel filtration buffer M400K10G. The cross-link reaction mixture was subjected to gel filtration on a Superdex 200 Increase column equilibrated with M400K10G buffer with 1 mM DTT at 0.3 ml/min flow rate. Peak fractions were analyzed by 8% SDS-PAGE and concentration determined with Bradford assay. Activity of each fraction was measured by the plate-reader unwinding assay.

Gel filtration of LC30

For the crosslinking reaction of UvrD S456C with the $MutL^{LC30}$ D452C fragment, full-length MutL D452C was treated with thrombin and $MutL^{LC30}$ was separated from $MutL^{LN40}$ by Size Exclusion chromatography. For this, 45 U of thrombin and 2 mM of DTT was added to 4.5 mg of MutL D452C and incubated ON in a dialysis bag with 14 kDa cut-off in M50K10G buffer. Samples were taken before and after cleavage and analyzed on 10% SDS-PAGE. The reaction mixture was filtered with a 0.22 μm Millipore filter and subjected to gel filtration on a Superdex 75 column equilibrated with M50K10G buffer with 1 mM DTT at 0.3 ml/min flow rate. All collected fractions were analyzed on a 10% SDS-PAGE and fractions containing pure $MutL^{LC30}$ fragment were pooled and concentrated with the protein concentrator (Vivaspin2, MWCO 10 k, Sartorius). $MutL^{LC30}$ concentration was measured spectrophotometrically and calculated by using theoretical coefficient. Aliquots (about 30 μM) were flash-frozen in liquid nitrogen and stored at −80 °C until further analysis.

CRediT authorship contribution statement

Olha Storozhuk: Writing – original draft, Visualization, Resources, Investigation, Formal analysis, Conceptualization. **Susanne R. Bruekner:** Writing – original draft, Visualization, Resources, Investigation, Formal analysis. **Ankon**

Paul: Resources, Investigation, Formal analysis. **Joyce H.G. Lebbink:** Writing – review & editing, Supervision, Funding acquisition. **Titia K. Sixma:** Writing – review & editing, Supervision, Funding acquisition, Conceptualization. **Peter Friedhoff:** Writing – review & editing, Writing – original draft, Visualization, Supervision, Funding acquisition, Conceptualization.

DECLARATION OF COMPETING INTEREST

The authors declare that they have no known competing financial interests or personal relationships that could have appeared to influence the work reported in this paper.

Acknowledgements

We thank Heike Büngen, Vladislav Kunetki, and Charlie Laffeber for experimental contributions in the early stage of the project. We thank T. Lohman for generous sharing of UvrD single cysteine plasmids. ChatGPT was used to improve wording in the introduction. This research was funded by the European Community's MSCA Horizon2020 project DNARepairMan [722433], NWO TOP 714.016.002, and gravitation program CancerGenomiCs.nl from the Netherlands Organisation for Scientific Research (NWO), part of the Oncode Institute, which is partly financed by the Dutch Cancer Society. Research at the Netherlands Cancer Institute is supported by institutional grants of the Dutch Cancer Society and of the Dutch Ministry of Health, Welfare and Sport.

Appendix A. Supplementary material

Supplementary material to this article can be found online at https://doi.org/10.1016/j.jmb.2024.168589.

Received 16 February 2024;
Accepted 19 April 2024;
Available online 25 April 2024

Keywords:
DNA mismatch repair;
helicase;
transient kinetics;
cross-linking

† CURE NF Research group, Medical Faculty, Martin Luther University Halle-Wittenberg, Halle (Saale), Germany, Große Steinstrasse 52, 06108 Halle (Saale), Germany.

References

1. Loeb, L.A., Loeb, K.R., Anderson, J.P., (2003). Multiple mutations and cancer. *Proc. Natl. Acad. Sci.* **100**, 776–781.
2. Fishel, R., Kolodner, R.D., (1995). Identification of mismatch repair genes and their role in the development of cancer. *Curr. Opin. Genet. Dev.* **5**, 382–395.
3. Kunkel, T.A., Erie, D.A., (2005). DNA mismatch repair*. *Annu. Rev. Biochem* **74**, 681–710.
4. Modrich, P., Lahue, R., (1996). Mismatch repair in replication fidelity, genetic recombination, and cancer biology. *Annu. Rev. Biochem* **65**, 101–133.
5. Fernandez-Leiro, R., Bhairosing-Kok, D., Kunetsky, V., Laffeber, C., Winterwerp, H.H., Groothuizen, F., et al., (2021). The selection process of licensing a DNA mismatch for repair. *Nature Struct. Mol. Biol.* **28**, 373–381.
6. Lamers, M.H., Perrakis, A., Enzlin, J.H., Winterwerp, H.H. K., de Wind, N., Sixma, T.K., (2000). The crystal structure of DNA mismatch repair protein MutS binding to a G·T mismatch. *Nature* **407**, 711–717.
7. Su, S.S., Modrich, P., (1986). Escherichia coli mutS-encoded protein binds to mismatched DNA base pairs. *Proc. Natl. Acad. Sci.* **83**, 5057–5061.
8. Groothuizen, F.S., Winkler, I., Cristóvão, M., Fish, A., Winterwerp, H.H.K., Reumer, A., et al., (2015). MutS/MutL crystal structure reveals that the MutS sliding clamp loads MutL onto DNA. *eLife* **4**, e06744.
9. Acharya, S., Foster, P.L., Brooks, P., Fishel, R., (2003). The coordinated functions of the *E. coli* MutS and MutL proteins in mismatch repair. *Mol. Cell* **12**, 233–246.
10. Allen, D.J., Makhov, A., Grilley, M., Taylor, J., Thresher, R., Modrich, P., et al., (1997). MutS mediates heteroduplex loop formation by a translocation mechanism. *EMBO J.* **16**, 4467–4476.
11. Grilley, M., Welsh, K.M., Su, S.S., Modrich, P., (1989). Isolation and characterization of the Escherichia coli mutl gene product. *J. Biol. Chem.* **264**, 1000–1004.
12. Lee, J.Y., Chang, J., Joseph, N., Ghirlando, R., Rao, D.N., Yang, W., (2005). MutH complexed with hemi- and unmethylated DNAs: Coupling base recognition and DNA cleavage. *Mol. Cell* **20**, 155–166.
13. Au, K.G., Welsh, K., Modrich, P., (1992). Initiation of methyl-directed mismatch repair. *J. Biol. Chem.* **267**, 12142–12148.
14. Lahue, R.S., Su, S.S., Modrich, P., (1987). Requirement for d(GATC) sequences in Escherichia coli mutHLS mismatch correction. *Proc. Natl. Acad. Sci.* **84**, 1482–1486.
15. Mechanic, L.E., Frankel, B.A., Matson, S.W., (2000). Escherichia coli MutL Loads DNA Helicase II onto DNA*. *J. Biol. Chem.* **275**, 38337–38346.
16. Yamaguchi, M., Dao, V., Modrich, P., (1998). MutS and MutL activate DNA Helicase II in a mismatch-dependent manner*. *J. Biol. Chem.* **273**, 9197–9201.
17. Hall, M.C., Jordan, J.R., Matson, S.W., (1998). Evidence for a physical interaction between the Escherichia coli methyl-directed mismatch repair proteins MutL and UvrD. *EMBO J.* **17**, 1535–1541.
18. Dao, V., Modrich, P., (1998). Mismatch-, MutS-, MutL-, and Helicase II-dependent unwinding from the single-strand break of an incised heteroduplex*. *J. Biol. Chem.* **273**, 9202–9207.

19. Viswanathan, M., Burdett, V., Baitinger, C., Modrich, P., Lovett, S.T., (2001). Redundant exonuclease involvement in Escherichia coli methyl-directed mismatch repair. *J. Biol. Chem.* **276**, 31053–31058.
20. Kadyrov, F.A., Genschel, J., Fang, Y., Penland, E., Edelmann, W., Modrich, P., (2009). A possible mechanism for exonuclease 1-independent eukaryotic mismatch repair. *PNAS* **106**, 8495–8500.
21. Goellner, E.M., Smith, C.E., Campbell, C.S., Hombauer, H., Desai, A., Putnam, C.D., et al., (2014). PCNA and Msh2-Msh6 activate an Mlh1-Pms1 endonuclease pathway required for Exo1-independent mismatch repair. *Mol. Cell* **55**, 291–304.
22. Liu, J., Lee, R., Britton, B.M., London, J.A., Yang, K., Hanne, J., et al., (2019). MutL sliding clamps coordinate exonuclease-independent Escherichia coli mismatch repair. *Nature Commun.* **10**, 5294.
23. Hermans, N., Laffeber, C., Cristovão, M., Artola-Borán, M., Mardenborough, Y., Ikpa, P., et al., (2016). Dual daughter strand incision is processive and increases the efficiency of DNA mismatch repair. *Nucleic Acids Res.* **44**, 6770–6786.
24. Iyer, R.R., Pluciennik, A., Burdett, V., Modrich, P.L., (2006). DNA mismatch repair: Functions and mechanisms. *Chem. Rev.* **106**, 302–323.
25. Lahue, R.S., Au, K.G., Modrich, P., (1989). DNA mismatch correction in a defined system. *Science* **245**, 160–164.
26. Guarné, A., Ramon-Maiques, S., Wolff, E.M., Ghirlando, R., Hu, X., Miller, J.H., et al., (2004). Structure of the MutL C-terminal domain: a model of intact MutL and its roles in mismatch repair. *EMBO J.* **23**, 4134–4145.
27. Drotschmann, K., Fritz, H.-J., Aronshtam, A., Marinus, M. G., (1998). The Escherichia coli MutL protein stimulates binding of Vsr and MutS to heteroduplex DNA. *Nucleic Acids Res.* **26**, 948–953.
28. Kosinski, J., Steindorf, I., Bujnicki, J.M., Giron-Monzon, L., Friedhoff, P., (2005). Analysis of the quaternary structure of the MutL C-terminal domain. *J. Mol. Biol.* **351**, 895–909.
29. Pillon, M.C., Lorenowicz, J.J., Uckelmann, M., Klocko, A. D., Mitchell, R.R., Chung, Y.S., et al., (2010). Structure of the endonuclease domain of MutL: Unlicensed to cut. *Mol. Cell* **39**, 145–151.
30. Ban, C., Junop, M., Yang, W., (1999). Transformation of MutL by ATP binding and hydrolysis: a switch in DNA mismatch repair. *Cell* **97**, 85–97.
31. Ban, C., Yang, W., (1998). Crystal structure and ATPase activity of MutL: implications for DNA repair and mutagenesis. *Cell* **95**, 541–552.
32. Sacho, E.J., Kadyrov, F.A., Modrich, P., Kunkel, T.A., Erie, D.A., (2008). Direct visualization of asymmetric adenine nucleotide-induced conformational changes in MutLα. *Mol. Cell* **29**, 112–121.
33. Giron-Monzon, L., Manelyte, L., Ahrends, R., Kirsch, D., Spengler, B., Friedhoff, P., (2004). Mapping protein-protein interactions between MutL and MutH by cross-linking. *J. Biol. Chem.* **279**, 49338–49345.
34. Sancar, A., (1996). DNA excision repair. *Annu. Rev. Biochem.* **65**, 43–81.
35. Veaute, X., Delmas, S., Selva, M., Jeusset, J., Cam, E.L., Matic, I., et al., (2005). UvrD helicase, unlike Rep helicase, dismantles RecA nucleoprotein filaments in Escherichia coli. *EMBO J.* **24**, 180–189.
36. Bruand, C., Ehrlich, S.D., (2000). UvrD-dependent replication of rolling-circle plasmids in Escherichia coli. *Mol. Microbiol.* **35**, 204–210.
37. Matson, S.W., George, J.W., (1987). DNA helicase II of Escherichia coli. Characterization of the single-stranded DNA-dependent NTPase and helicase activities. *J. Biol. Chem.* **262**, 2066–2076.
38. Tomko, E.J., Lohman, T.M., (2017). Modulation of Escherichia coli UvrD single-stranded DNA translocation by DNA base composition. *Biophys. J* . **113**, 1405–1415.
39. Matson, S.W., (1986). Escherichia coli helicase II (urvD gene product) translocates unidirectionally in a 3' to 5' direction. *J. Biol. Chem.* **261**, 10169–10175.
40. Mechanic, L.E., Hall, M.C., Matson, S.W., (1999). Escherichia coli DNA Helicase II Is active as a monomer*. *J. Biol. Chem.* **274**, 12488–12498.
41. Ali, J.A., Maluf, N.K., Lohman, T.M., (1999). An oligomeric form of E. coli UvrD is required for optimal helicase activity. *J. Mol. Biol.* **293**, 815–834.
42. Fischer, C.J., Maluf, N.K., Lohman, T.M., (2004). Mechanism of ATP-dependent translocation of E. coli UvrD monomers along single-stranded DNA. *J. Mol. Biol.* **344**, 1287–1309.
43. Lohman, T.M., Tomko, E.J., Wu, C.G., (2008). Non-hexameric DNA helicases and translocases: mechanisms and regulation. *Nature Rev. Mol. Cell Bio.* **9**, 391–401.
44. Runyon, G.T., Lohman, T.M., (1989). Escherichia coli Helicase II (UvrD) protein can completely unwind fully duplex linear and nicked circular DNA. *J. Biol. Chem.* **264**, 17502–17512.
45. Runyon, G.T., Bear, D.G., Lohman, T.M., (1990). Escherichia coli helicase II (UvrD) protein initiates DNA unwinding at nicks and blunt ends. *Proc. Natl. Acad. Sci.* **87**, 6383–6387.
46. Maluf, N.K., Fischer, C.J., Lohman, T.M., (2003). A dimer of Escherichia coli UvrD is the active form of the helicase in vitro. *J. Mol. Biol.* **325**, 913–935.
47. Ordabayev, Y.A., Nguyen, B., Niedziela-Majka, A., Lohman, T.M., (2018). Regulation of UvrD helicase activity by MutL. *J. Mol. Biol.* **430**, 4260–4274.
48. Lee, J.Y., Yang, W., (2006). UvrD helicase unwinds DNA one base pair at a time by a two-part power stroke. *Cell* **127**, 1349–1360.
49. Sanders, K., Lin, C.-L., Smith, A.J., Cronin, N., Fisher, G., Eftychidis, V., et al., (2017). The structure and function of an RNA polymerase interaction domain in the PcrA/UvrD helicase. *Nucleic Acids Res.* **45**, gkx074.
50. Kawale, A.A., Burmann, B.M., (2020). UvrD helicase–RNA polymerase interactions are governed by UvrD's carboxy-terminal Tudor domain. *Commun. Biol.* **3**, 607.
51. Gwynn, E.J., Smith, A.J., Guy, C.P., Savery, N.J., McGlynn, P., Dillingham, M.S., (2013). The conserved C-terminus of the PcrA/UvrD helicase interacts directly with RNA polymerase. *PLoS One* **8**, e78141.
52. Chadda, A., Kozlov, A.G., Nguyen, B., Lohman, T.M., Galburt, E.A., (2023). Mycobacterium tuberculosis Ku stimulates multi-round DNA unwinding by UvrD1 monomers. *J. Mol. Biol.* **436**, 168367
53. Korolev, S., Hsieh, J., Gauss, G.H., Lohman, T.M., Waksman, G., (1997). Major domain swiveling revealed by the crystal structures of complexes of E. coli rep helicase bound to single-stranded DNA and ADP. *Cell* **90**, 635–647.
54. Jia, H., Korolev, S., Niedziela-Majka, A., Maluf, N.K., Gauss, G.H., Myong, S., et al., (2011). Rotations of the 2B sub-domain of E. coli UvrD helicase/translocase coupled to nucleotide and DNA binding. *J. Mol. Biol.* **411**, 633–648.

55. Nguyen, B., Ordabayev, Y., Sokoloski, J.E., Weiland, E., Lohman, T.M., (2017). Large domain movements upon UvrD dimerization and helicase activation. *Proc. Natl. Acad. Sci. U.S.A.* **114**, 12178–12183.
56. Ordabayev, Y.A., Nguyen, B., Kozlov, A.G., Jia, H., Lohman, T.M., (2019). UvrD helicase activation by MutL involves rotation of its 2B subdomain. *Proc. Natl. Acad. Sci.* **116**, 16320–16325.
57. Comstock, M.J., Whitley, K.D., Jia, H., Sokoloski, J., Lohman, T.M., Ha, T., et al., (2015). Direct observation of structure-function relationship in a nucleic acid–processing enzyme. *Science* **348**, 352–354.
58. Ma, W., Whitley, K.D., Chemla, Y.R., Luthey-Schulten, Z., Schulten, K., (2018). Free-energy simulations reveal molecular mechanism for functional switch of a DNA helicase. *Elife* **7**, e34186.
59. Cheng, W., Brendza, K.M., Gauss, G.H., Korolev, S., Waksman, G., Lohman, T.M., (2002). The 2B domain of the Escherichia coli Rep protein is not required for DNA helicase activity. *Proc. Natl. Acad. Sci.* **99**, 16006–16011.
60. Brendza, K.M., Cheng, W., Fischer, C.J., Chesnik, M.A., Niedziela-Majka, A., Lohman, T.M., (2005). Autoinhibition of Escherichia coli Rep monomer helicase activity by its 2B subdomain. *Proc. Natl. Acad. Sci.* **102**, 10076–10081.
61. Niedziela-Majka, A., Maluf, N.K., Antony, E., Lohman, T. M., (2011). Self-assembly of Escherichia coli MutL and its complexes with DNA. *Biochemistry* **50**, 7868–7880.
62. Loo, T.W., Clarke, D.M., (2001). Determining the dimensions of the drug-binding domain of human P-glycoprotein using thiol cross-linking compounds as molecular rulers*. *J. Biol. Chem.* **276**, 36877–36880.
63. Borsellini, A., Lebbink, J.H.G., Lamers, M.H., (2022). MutL binds to 3′ resected DNA ends and blocks DNA polymerase access. *Nucleic Acids Res.* **50**, 6224–6234.
64. Mauris, J., Evans, T.C., (2010). A human PMS2 homologue from aquifex aeolicus stimulates an ATP-dependent DNA helicase. *J. Biol. Chem.* **285**, 11087–11092.
65. Zundert, G.C.P.V., Rodrigues, J.P.G.L.M., Trellet, M., Schmitz, C., Kastritis, P.L., Karaca, E., et al., (2016). The HADDOCK2.2 web server: User-friendly integrative modeling of biomolecular complexes. *J. Mol. Biol.* **428**, 720–725.
66. Honorato, R.V., Koukos, P.I., Jiménez-García, B., Tsaregorodtsev, A., Verlato, M., Giachetti, A., et al., (2021). Structural biology in the clouds: The WeNMR-EOSC ecosystem. *Front. Mol. Biosci.* **8**, 729513
67. Evans, R., Oeill, M., Pritzel, A., Antropova, N., Senior, A., Green, T., et al., (2022). Protein complex prediction with AlphaFold-Multimer. *bioRxiv* 2021.10.04.463034.
68. Mirdita, M., Schütze, K., Moriwaki, Y., Heo, L., Ovchinnikov, S., Steinegger, M., (2022). ColabFold: making protein folding accessible to all. *Nature Methods* **19**, 679–682.
69. Jumper, J., Evans, R., Pritzel, A., Green, T., Figurnov, M., Ronneberger, O., et al., (2021). Highly accurate protein structure prediction with AlphaFold. *Nature* **596**, 583–589.
70. Maluf, N.K., Ali, J.A., Lohman, T.M., (2003). Kinetic mechanism for formation of the active, dimeric UvrD helicase-DNA complex*. *J. Biol. Chem.* **278**, 31930–31940.
71. Glaser, F., Pupko, T., Paz, I., Bell, R.E., Bechor-Shental, D., Martz, E., et al., (2003). ConSurf: Identification of functional regions in proteins by surface-mapping of phylogenetic information. *Bioinformatics* **19**, 163–164.
72. Worth, C.L., Preissner, R., Blundell, T.L., (2011). SDM—a server for predicting effects of mutations on protein stability and malfunction. *Nucleic Acids Res.* **39**, W215–W222.
73. Chen, C.-W., Lin, J., Chu, Y.-W., (2013). iStable: off-the-shelf predictor integration for predicting protein stability changes. *BMC Bioinform.* **14**, S5.
74. Feng, G., Winkler, M.E., (1995). Single-step purifications of His6-MutH, His6-MutL and His6-MutS repair proteins of escherichia coli K-12. *Biotechniques* **19**, 956–965.
75. Natrajan, G., Lamers, M.H., Enzlin, J.H., Winterwerp, H.H. K., Perrakis, A., Sixma, T.K., (2003). Structures of Escherichia coli DNA mismatch repair enzyme MutS in complex with different mismatches: a common recognition mode for diverse substrates. *Nucleic Acids Res.* **31**, 4814–4821.
76. Runyon, G.T., Wong, I., Lohman, T.M., (1993). Overexpression, purification, DNA binding, and dimerization of the Escherichia coli uvrD gene product (helicase II). *Biochemistry* **32**, 602–612.
77. Nørby, J.G., (1988). Coupled assay of Na+, K+-ATPase activity. *Methods Enzym.* **156**, 116–119.
78. Schindelin, J., Arganda-Carreras, I., Frise, E., Kaynig, V., Longair, M., Pietzsch, T., et al., (2012). Fiji: an open-source platform for biological-image analysis. *Nature Methods* **9**, 676–682.